Nuclear Instruments and Methods in Physics Research A 1076 (2025) 170496

Contents lists available at ScienceDirect

Nuclear Inst. and Methods in Physics Research, A

journal homepage: www.elsevier.com/locate/nima

Full Length Article

Integration of the FastIC front-end electronics into the Picosec MicroMegas detector

L. Scharenberg [a,*], J. Alozy [a], Y. Angelis [b,c], S. Aune [d], R. Ballabriga [a], J. Bortfeldt [e], F. Brunbauer [a], M. Brunoldi [f,g], M. Campbell [a], J. Datta [h], R. De Oliveira [a], K. Dehmelt [i], G. Fanourakis [j], J.M. Fernandez-Tenllado [a,k], K.J. Flöthner [a,l], D. Fiorina [f,g], M. Gallinaro [m], F. Garcia [n], D. Gascon [k], I. Giomataris [d], K. Gnanvo [i], S. Gomez [o,k], F.J. Iguaz [d,1], D. Janssens [a], A. Kallitsopoulou [d], M. Kovacic [p], B. Kross [i], P. Legou [d], M. Lisowska [a,q], J. Liu [r], M. Lupberger [l,s], R. Manera [k], I. Maniatis [a,b,2], A. Mariscal [k], J. Mauricio [k], J. McKisson [i], Y. Meng [r], H. Muller [s,a], E. Oliveri [a], G. Orlandini [a,t], A. Pandey [i], T. Papaevangelou [d], E. Picatoste [k], M. Piller [a,u], M. Pomorski [v], L. Ropelewski [a], D. Sampsonidis [b,c], A. Sanuy [k], T. Schneider [a], E. Scorsone [v], L. Sohl [d,3], M. van Stenis [a], Y. Tsipolitis [w], S.E. Tzamarias [b,c], A. Utrobicic [x], I. Vai [f,g], R. Veenhof [a], P. Vitulo [f,g], X. Wang [r], S. White [y], W. Xi [i], Z. Zhang [r], Y. Zhou [r]

[a] European Organization for Nuclear Research (CERN), 1211 Geneva 23, Switzerland
[b] Department of Physics, Aristotle University of Thessaloniki, University Campus, 54124 Thessaloniki, Greece
[c] Center for Interdisciplinary Research and Innovation (CIRI-AUTH), Thessaloniki 57001, Greece
[d] Institut de Recherche sur les lois Fondamentales de l'Univers (IRFU, CEA), Université Paris-Saclay, F-91191 Gif-sur-Yvette, France
[e] Department for Medical Physics, Ludwig Maximilian University of Munich, Am Coulombwall 1, 85748 Garching, Germany
[f] Dipartimento di Fisica, Università di Pavia, Via Bassi 6, 27100 Pavia, Italy
[g] INFN Sezione di Pavia, Via Bassi 6, 27100 Pavia, Italy
[h] Department of Physics and Astronomy, Stony Brook University, Stony Brook, NY 11794-3800, United States
[i] Thomas Jefferson National Accelerator Facility (Jefferson Lab), 12000 Jefferson Avenue, Newport News, VA 23606, United States
[j] Institute of Nuclear and Particle Physics, NCSR "Demokritos", P.O. Box 60037, 15310 Agia Paraskevi, Greece
[k] Institute of Cosmos Sciences (ICCUB), University of Barcelona, Martí Franquès 1, 08028 Barcelona, Spain
[l] Helmholtz-Institut für Strahlen- und Kernphysik, University of Bonn, Nußallee 14-16, 53115 Bonn, Germany
[m] Laboratório de Instrumentação e Física Experimental de Partículas (LIP), Av. Prof. Gama Pinto 2, 1649-003 Lisbon, Portugal
[n] Helsinki Institute of Physics, University of Helsinki, P.O. Box 64, FI-00014, Finland
[o] Serra Hunter Fellow, Electronics Department, Polytechnic University of Catalonia (UPC), Eduard Maristany 16, 08019 Barcelona, Spain
[p] University of Zagreb, Faculty of Electrical Engineering and Computing, Unska 3, 10000 Zagreb, Croatia
[q] Université Paris-Saclay, F-91191 Gif-sur-Yvette, France
[r] State Key Laboratory of Particle Detection and Electronics, University of Science and Technology of China (USTC), Hefei 230026, China
[s] Physikalisches Institut, University of Bonn, Nußallee 12, 53115 Bonn, Germany
[t] Friedrich-Alexander-Universität Erlangen-Nürnberg, Schloßplatz 4, 91054 Erlangen, Germany
[u] Institute of Electronics, Graz University of Technology, Inffeldgasse 12/I, 8010 Graz, Austria
[v] Laboratory for Integration of Systems and Technology (CEA-LIST), Diamond Sensors Laboratory, CEA Saclay, F-91191 Gif-sur-Yvette, France
[w] National Technical University of Athens, 106 82, Athens, Greece
[x] Ruder Bošković Institute, Bijenička cesta 54, 10000 Zagreb, Croatia
[y] Department of Physics, University of Virginia, P.O. Box 400714, Charlottesville, VA 22904-4714, United States

ARTICLE INFO

Keywords:
Gaseous fast-timing detectors

ABSTRACT

The Picosec MicroMegas collaboration aims to develop gaseous fast-timing detectors; experimentally, intrinsic time resolutions from around 50 ps to better than 20 ps are obtained, depending on the exact detector

* Corresponding author.
E-mail address: lucian.scharenberg@cern.ch (L. Scharenberg).
[1] Now at: Synchrotron SOLEIL, L'Orme des Merisiers, Départementale 128, 91190 Saint-Aubin, France.
[2] Now at: Department of Particle Physics and Astronomy, Weizmann Institute of Science, 234 Herzl Street, P.O. Box 26, Rehovot 76100, Israel.
[3] Now at: TÜV NORD EnSys GmbH & Co. KG, Germany.

https://doi.org/10.1016/j.nima.2025.170496
Received 16 September 2024; Received in revised form 28 March 2025; Accepted 31 March 2025
Available online 12 April 2025

Picosec MicroMegas
FastIC
Precise timing electronics

configuration. Parts of developments focus on exploring various options of fast-timing multi-channel front-end electronics, to meet the data processing demands of experimental applications. One option is the FastIC, which was developed for reading out positive and negative input polarity sensors with intrinsic amplification. In this paper, the first results from reading out the gaseous Picosec MicroMegas detector with the FastIC are presented. In laboratory studies, a basic description of the data processing chain was performed using a function generator. The results from test beam measurements are used to characterise the timing performance and the charge processing of the combination of FastIC and Picosec MicroMegas, as well as to demonstrate the possibility of a multi-channel detector readout. Although the timing-at-threshold level of the FastIC introduces a time walk of around 1.5 ns, time resolutions of around 50 ps have been achieved.

1. Introduction

Current and future accelerator experiments [1] require large-area fast-timing detectors to reduce pile-up events. For example, in case of the High-Luminosity LHC upgrades, time resolutions of better than 30 ps are needed [2,3]. Driven by these needs, the Picosec MicroMegas [4] collaboration is developing large-area (currently individual modules with $10 \times 10\,\text{cm}^2$ active area with 100 readout channels) gaseous fast-timing detectors. Depending on the detector configuration (Section 3), time resolutions from around 50 ps to below 20 ps [5] can be achieved.

Technologically, the Picosec MicroMegas (MM) detector concept provides various advantages that could be interesting for future experimental applications. As such, the ongoing studies on using eco-friendly gases should be mentioned [6], as well as the ability to achieve 10's of picosecond time resolution while applying maximally several hundreds of volts for the drift/pre-amplification (see Section 3) and signal amplification. Also, the ability to use a Picosec MicroMegas detector as a single-photon detection device is of interest to various applications. In addition, preliminary tests showed a successful operation at $100\,\text{kHz/cm}^2$ interaction rate.

When optimising the various Picosec MM prototype detectors, the signal waveforms are usually acquired with high-bandwidth oscilloscopes. While this method provides excellent information about the detector behaviour, it is not feasible for possible future experimental applications, requiring a large number of readout channels. The combination of a large channel count and high-rate requirements makes the use of dedicated multi-channel front-end electronics obligatory. Hence, the Picosec MicroMegas collaboration also explores different types of multi-channel front-end electronics that can be combined with the detectors.

As an example of these efforts, the ongoing studies [7] with the SAMPIC digitiser [8] or the DRS4 electronics [9] can be mentioned, which aim for a full sampling and offline fitting of the detector's signal waveforms. Another example, which is presented in this paper, is the FastIC [10,11], which aims for a binary output providing directly the Signal Arrival Time (SAT) — based on a leading edge discriminator — and the signal amplitude. Currently, this binary output requires further digitisation by a Time to Digital Converter (TDC). In the future, a TDC will be integrated into the succeeding FastIC+ Application-Specific Integrated Circuit (ASIC). This future on-chip digitisation is also one of the main advantages of the readout chain with FastIC, as it does not require any offline waveform analysis but directly provides a digital output with all the required information. Without transmitting the full waveform, also the rate-capability is sufficiently high, with up to 2 MHz hit rate per channel in case the energy information is required or up to 50 MHz if the application allows to omit it.

Here, the first results from using the FastIC front-end electronics (Section 2) with a Picosec MM detector are presented. This includes the electronics' characterisation with a function generator, as well as the first results from test beam measurements, showing — despite a slight degradation in time resolution — the general applicability of the FastIC for the application in the Picosec MicroMegas (Sections 6 and 7). While these measurements were performed on the level of a single readout channel, also test beam studies with a multi-channel readout have been performed to demonstrate the applicability for experiments (Section 9).

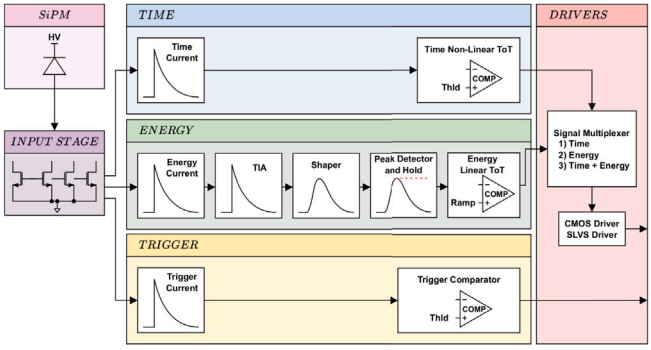

Fig. 1. Block diagram of the FastIC. For the presented measurements, the detector was not a Silicon PhotoMultiplier (SiPM), but a Picosec MicroMegas detector. Figure taken from [11].

2. The FastIC front-end ASIC

The FastIC is an 8-channel front-end ASIC, designed by the University of Barcelona and CERN for generic fast-timing applications, employing positive or negative input polarity sensors with intrinsic amplification [10–12]. The readout channels require current signals as input and provide a dynamic range of about 5 µA to 20 mA peak current. The signal processing is configured as follows to operate with the Picosec MM detectors. At the input stage, a MOSFET current mirror with a double feedback loop is used, similar to the one developed for the HRFlexTOT ASIC [13]. The signal current from the detector is copied through the current mirrors[4] into the three output branches of the FastIC input stage, each branch dedicated to time, energy, or trigger outputs (Fig. 1). In the timing branch, the detector current is directly processed by a comparator with an adjustable Threshold Level (THL), defining the Signal Arrival Time (SAT) as the time when the detector current crosses the THL. In the energy branch, the current is first processed by a Trans-Impedance Amplifier (TIA), followed by a shaper with configurable peaking time — either 5 ns or as here 25 ns — and a peak detector.

In the chosen operation mode, both types of information are provided as two consecutive pulses of a binary signal (see Section 6 and Fig. 12(a) for an example). The first pulse, with fixed length, referred to as the time signal, encodes the SAT in the rising edge of the pulse. The second pulse encodes the energy response using a pulse width modulation, where the detected peak amplitude of the shaper output is modulated by the width of this pulse [11]. In these studies, the binary signals were acquired with an oscilloscope, followed by an offline analysis, due to ongoing implementation of a TDC into the FastIC that would provide a full digital output. The third branch is dedicated to triggering purposes but was not utilised in the presented studies.

For the measurements, a FastIC 16 channel testing board was used, combining two ASICs on a single evaluation board. The testing board

[4] For a full description of the current mirror circuit on the transistor-level, it is referred to [13].

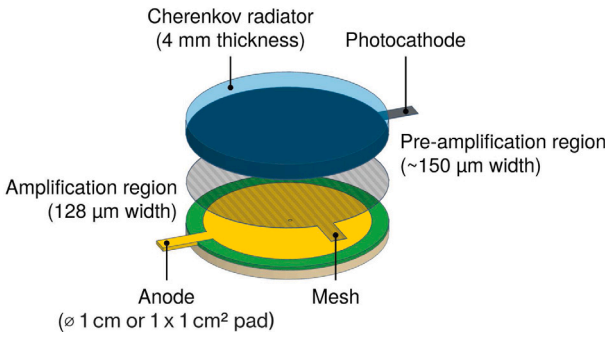

Fig. 2. Simplified illustration of a typical single-channel Picosec MicroMegas detector (not drawn to scale).

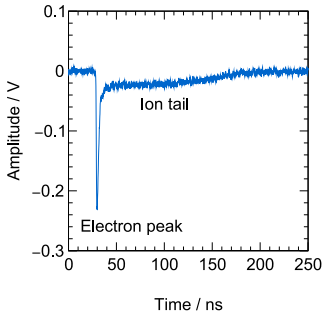

Fig. 3. Exemplary waveform of a charge signal induced in the 1 cm diameter readout pad of the prototype detector used for the here presented measurements. The shown waveform is not the raw detector signal, but it is amplified by a Cividec C2 current amplifier, before being acquired with an oscilloscope (Teledyne LeCroy Waverunner 8104).

allows several ways of injecting a signal into the FastIC, with a Hirose connector being the one used here. In addition, various other connectors are provided, to access the analogue response of the TIA, the shaper and the peak detector.

3. The Picosec MicroMegas detector

A Picosec MM [4] is a gaseous detector filled with a gas mixture of $Ne/C_2H_6/CF_4$ (80/10/10%), combining a bulk MicroMegas with a 128 µm amplification gap with a 3–5 mm thick magnesium fluoride (MgF_2) Cherenkov radiator (Fig. 2). Sputtered on the radiator is a photocathode. Following the passage of a high-energetic particle through the Cherenkov radiator, UV photons are created which release photoelectrons from the photocathode. The drift region itself serves as a pre-amplification region, with a reduced width from a typically millimetre-scale to 120 and 220 µm. This configuration reduces the otherwise occurring time-jitter of the primary ionisation in the drift region of a gaseous detector.

The charge signal induced in the readout electrodes of MicroMegas-like detectors [14] shows a characteristic behaviour, defined by the movement of the charge carriers in the amplification stage (Fig. 3). At first, there is the so-called 'electron peak', caused by the electrons of the amplifications' avalanche drifting fast towards the readout anode, followed by the longer 'ion tail', caused by the ions from the avalanche drifting slowly away from the electrode towards the MM mesh. An essential part of the standard Picosec MM operation is to measure these waveforms after being processed by a current amplifier that is connected between the detector and the oscilloscope. The amplifier enables better visualisation of the waveform on the oscilloscope and allows to employ the full dynamic range of the oscilloscope's ADC. Furthermore, the amplifier acts as a filter and thus improves the signal-to-noise ratio. Two amplifier models are used: either the commercially available Cividec C2 40 dB Broadband Amplifier or a custom-made 38.5 dB current pre-amplifier with 44 Ω input impedance [15] that is based on an amplifier circuit for diamond-based detectors [16].

4. Low amplitude signals

While the amplifiers are used in the default measurements, as well as in the ones with the SAMPIC, one of the aspects investigated during the detector-electronics-integration was the FastIC's response to low amplitude signals. Here, it should be noted that in the timing branch of the FastIC, no amplification takes place. Hence, these measurements served mainly to understand the possibility to operate the system without the need of the additional amplifiers — with the dynamic range of the FastIC starting at around 5 µA peak current this should be theoretically possible. To investigate this, an almost Gaussian pulse has been generated from a rectangular pulse from a function generator (Tektronix AFG3252) sent to a capacitor (Fig. 4).

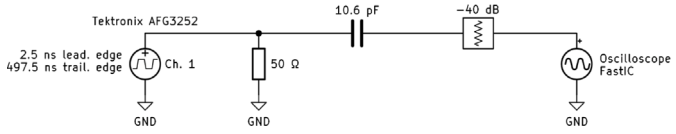

Fig. 4. Schematics of the circuit used to generate the low amplitude signals. Before being injected into the FastIC, the pulse was attenuated with a 40 dB attenuator, as the function generator was limited in the lowest possible amplitude.

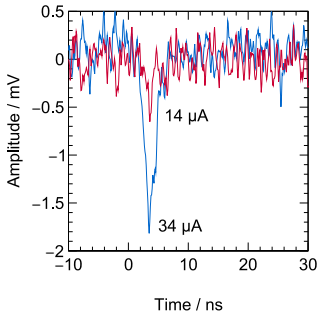

Fig. 5. Examples of the low amplitude pulses, injected into the FastIC. The annotated current values have been derived from the amplitude, with the input lines being 50 Ω terminated.

The first point that can be derived from these studies becomes directly visible from the pulses shown in Fig. 5: despite the dynamic range starting at around 5 µA, the minimum input current needs to be larger — here greater than around 17 µA, which corresponds to the set THL for the following measurements — due to electronic noise. The second point is derived from the measurements of the detection efficiency of the FastIC's input stage. The pulses were sent with a frequency of 10 kHz. Then the frequency of the processed pulses was measured, with the ratio of these two numbers giving the efficiency, depending on the bias current settings of the input stage (Fig. 6(a)). A larger bias current — reflected by a smaller Digital-to-Analogue-Converter (DAC) value — leads to a higher bandwidth of the input and thus increases the probability of the signal detection and processing. This was measured for different peak amplitudes, showing that around 34 µA peak current are needed to be fully efficient. A second measurement (Fig. 6(b)), with the attenuator and the capacitance being swapped in their order in the pulsing scheme (Fig. 4), shows a better behaviour, with inefficiencies only appearing at low bias currents. It should be noted that while the reason for the difference between the two runs is not completely understood, it shows the sensitivity in the processing of low amplitude signals. Hence, to be less sensitive

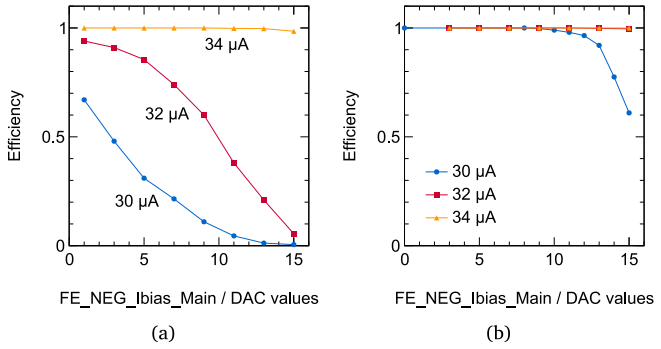

Fig. 6. Efficiency of the FastIC's input stage to test pulses with different peak amplitudes, depending on the DAC settings of the bias current of the input stage. A smaller DAC value is related to a higher bias current. In (a), the results of the first measurement are shown. In (b), the results obtained from a second measurement, performed a few months after the first one, with the order of the 10.6 pF capacitor and the 40 dB attenuator (Fig. 4) being swapped, are shown.

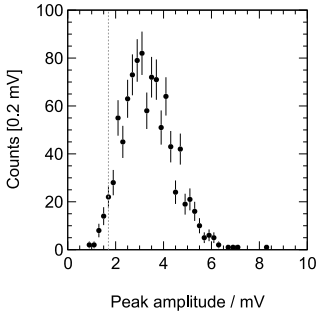

Fig. 7. Distribution of the peak amplitudes from the Picosec waveform, recorded with a single channel detector during the test beam campaigns (Section 5.2), with the cathode voltage set to 540 V. The peak amplitudes have been divided by the amplification factor of the additional current amplifier, to correspond to the amplitude of the actual detector signals.

to the observed fluctuations and to ensure a fully efficient operation at low detector gains, the FastIC measurements have been performed with additional signal amplification, using the custom 38.5 dB current pre-amplifier [15].

The benefit of using additional amplification becomes even more evident, when comparing the obtained pulser results with the measured amplitude distribution of the electron peak of the Picosec waveform (Fig. 7). The dashed line in Fig. 7 indicates where a peak current of 34 µA would correspond to in voltage. In the given example, the detector was operated at very high gain settings of $> 10^6$. Even at these values, small inefficiencies can be expected, as seen by all the entries left of the dashed line, which is a behaviour that is more prevalent at lower detector gain settings.

5. Experimental methods

In the following the experimental methods and set-ups are presented for the characterisation of the detector-front-end-integration. On the one hand, the energy response is studied, i.e. how the charge information from the Picosec waveform with an electron peak of around 2 ns length and ion tail of around 150 ns length is preserved after being processed by a shaper with 25 ns peaking time. These aspects have been mainly studied with well-defined test pulses from a function generator (Section 5.1). On the other hand, time resolution measurements, the detector efficiency, as well as the multi-channel readout, have been all studied in test beam campaigns with a beam telescope (Section 5.2).

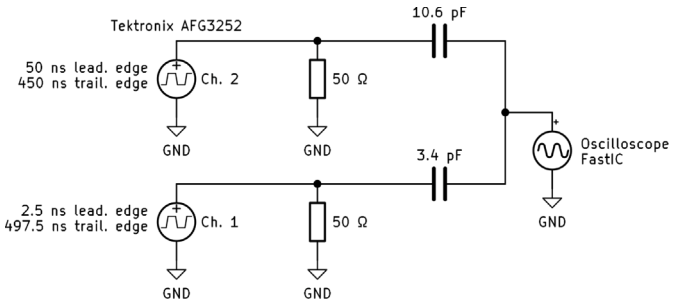

Fig. 8. Schematics of the circuit used to generate the emulated Picosec waveform. On each of the two channels of the generator, a 10 µs long square pulse was generated with a frequency of 10 kHz. Channel 1 was used to generate the electron peak signal, while channel 2 was used for the ion tail.

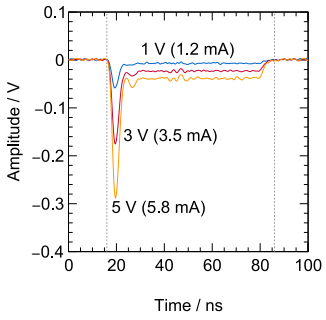

Fig. 9. Emulated Picosec waveforms, sent into the FastIC input, for different amplitude settings of the function generator. The number in parentheses corresponds to the peak current. The vertical dashed lines indicate the integral boundaries for calculating the amount of injected charge.

5.1. Studies with a function generator

At first, the response of the energy branch — because of required time walk corrections (Section 7) — on the Picosec waveform (Fig. 3) was studied, by emulating the waveform with a function generator (Tektronix AFG3252) and directly injecting it into a single readout channel (Fig. 8). Due to the need for an amplifier — indicated by the previously shown measurements — the emulated waveform (Fig. 9) corresponds to the one after amplification. For the subsequent studies, the total injected charge of the emulated waveforms, which is processed by the FastIC's energy branch, was determined by taking the integral within a fixed time interval, indicated by the dashed lines in Fig. 9. This allows to investigate the energy branch's behaviour depending on the injected charge and not the amplitude settings of the function generator. The results of these studies are presented in Section 6.1.

5.2. Test beam setup

For the performance evaluation of a Picosec MM with FastIC readout, two detector prototypes were operated during a test beam campaign at the H4 beam line of the Super Proton Synchrotron (SPS) at CERN, recording the interactions of 120 GeV/c muons. The Devices Under Test (DUTs) were mounted within a beam telescope, as sketched in Fig. 10. A Micro-Channel Plate Photo-Multiplier Tube (MCP-PMT, Hamamatsu R3809U-50) with a measured time resolution of around 5 ps serves as the timing reference. In addition, three COMPASS-like triple-GEM detectors [17] with X-Y-strip readout anode and around 60 µm spatial resolution are mounted in the beam telescope to provide the position of the interacting particle within the Picosec detectors. The GEM detectors are read out using APV25/SRS [18], which is triggered by the MCP-PMT. This trigger information serves then also as a reference for detector efficiency studies.

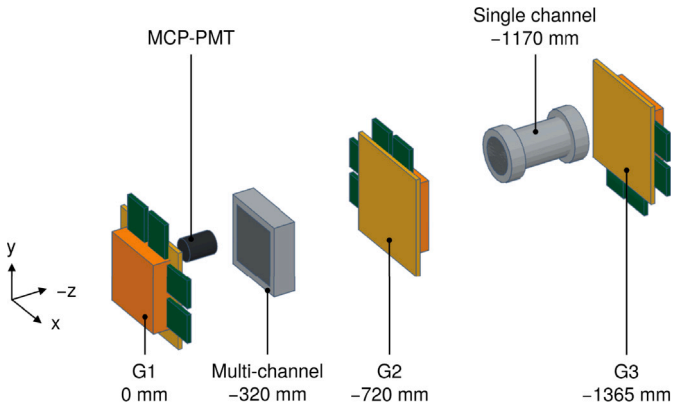

Fig. 10. Sketch of the beam telescope's components. Three COMPASS-like triple-GEM detectors (labelled G1, G2 and G3 in the sketch) are used to provide a reference position. An MCP-PMT is used to provide the reference time. In addition, it contains the two detectors under test (labelled 'Multi-channel' and 'Single channel' in the sketch), which are read out with the FastIC. The numbers under each detector label indicate the relative position within the beam telescope with respect to the first detector, which is tracking detector G1 at the 0 mm position. The total lever arm of the beam telescope is around 1.4 m.

The first DUT is a detector with a single circular readout pad of 1 cm diameter, 150 µm pre-amplification gap and CsI photocathode. Its main application was to collect reference data, using the default Picosec DAQ chain consisting of a Cividec C2 40 dB broadband current amplifier and a high-bandwidth oscilloscope and 10 GS/s sampling rate (Teledyne LeCroy Waverunner 8104) for acquiring waveforms. Offline waveform fitting would subsequently take place, in addition to the collection of comparison data using the binary output from the FastIC. It has to be noted that the binary output of the FastIC was acquired with the same oscilloscope, because of inability to covert the pulses into a data format processable by a DAQ computer. The acquired data sets allow comparing the time resolution and detector efficiency, depending on different field configurations. The anode voltage was fixed to +275 V, the mesh was grounded, and the cathode voltage was varied around −500 V.

The second DUT is a large area multi-channel detector with $10 \times 10\,\text{cm}^2$ active area and 100 square readout pads with $1\,\text{cm}^2$ pad area. The pre-amplification gap was 180 µm wide, again with a CsI photocathode. The anode voltage was kept at +275 V, while the cathode voltage was set to −520 V. Its application for the presented studies was to demonstrate the multi-channel readout capability of the FastIC. The results of the test beam studies are presented in Section 6.2 for the charge processing, Section 7 for time resolution results, 8 for the efficiency studies, as well as Section 9 for the multi-channel studies.

6. Charge processing

Given that the peaking time of the FastIC's shaper is too short for a full integration of the Picosec MM signal, the processing of such a signal type by the FastIC's energy branch needs investigation, for the time walk correction in the time resolution studies. This requires confirming the proportionality between the input charge and the amplitude of the output signal.

6.1. Function generator

With the well-defined emulated Picosec waveforms (Fig. 9) being directly injected into the FastIC, the corresponding shaper output (Fig. 11(a)) can be studied via the response of the energy branch. For this, the relation between the total injected charge and the peak amplitude of the shaper output (Fig. 11(b)) is plotted. To determine the total injected charge, the integral of the waveforms was taken in the range indicated by the dashed lines (Fig. 9). The peak amplitude of the shaper output is defined as the distance between baseline and the maximum value of the waveform after being processed by a moving average to reduce the noise contribution. Fitted to the data points in Fig. 11(b) is a linear function, confirming the required linearity between input charge and charge processing in the FastIC.

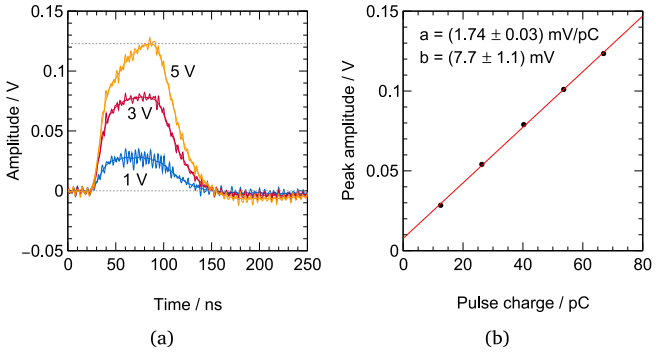

Fig. 11. In (a), the signal amplitude of the shaper output for the different input pulses (see Fig. 9) is shown. The horizontal dashed lines indicate the baseline and the peak of the shaper output to determine the peak amplitude. In (b), the linearity of the peak amplitude with respect to the input charge is shown.

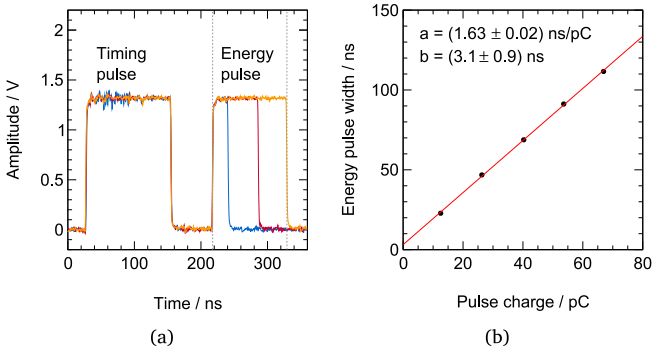

Fig. 12. In (a), the digital signal output of the FastIC for the different injected pulses is shown. The vertical dashed lines indicate the position of the rising and falling edge of the energy pulse at the 50 % amplitude level, used to determine its width. In (b), the linearity of the energy pulse's width with respect to the input charge is shown.

As the width of the energy pulse is supposed to be linearly proportional to the shaper peak amplitude, also the relation between the width and the injected charge was investigated to confirm proportionality. Also here, the response to different input charges was studied (Fig. 12(a)). As expected, the linearity between input and output could be confirmed with a linear fit (Fig. 12(b)).

6.2. Test beam

After establishing the linearity with test pulses, the results were confirmed with test beam measurements. As with the previous measurements, both, the shaper output, as well as the energy pulse width are monitored. They are compared to the electron peak charge measured after the Cividec amplifier. One of the first observations is a change in the shaper response: instead of a broad output pulse with a larger peaking time (Fig. 11, test pulse measurements), the peaking time remains at the design value of around 25 ns (Fig. 13, beam measurements), followed by an undershoot of the waveform. It was found that the different coupling between the custom amplifier or the function generator and the FastIC has an effect on the shape of the analogue output signal. However, this would explain only the shorter peak pulse but not the undershoot. This can be explained by the shorter rise and decay time of the electron

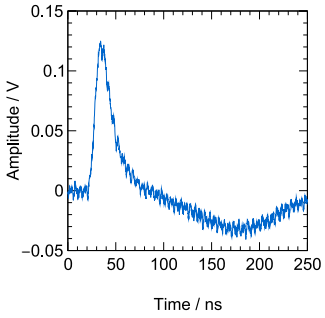

Fig. 13. Example of the shaper output, with an actual Picosec MM waveform as depicted in Fig. 3 as input signal and not an emulated waveform with longer rise time (Fig. 9).

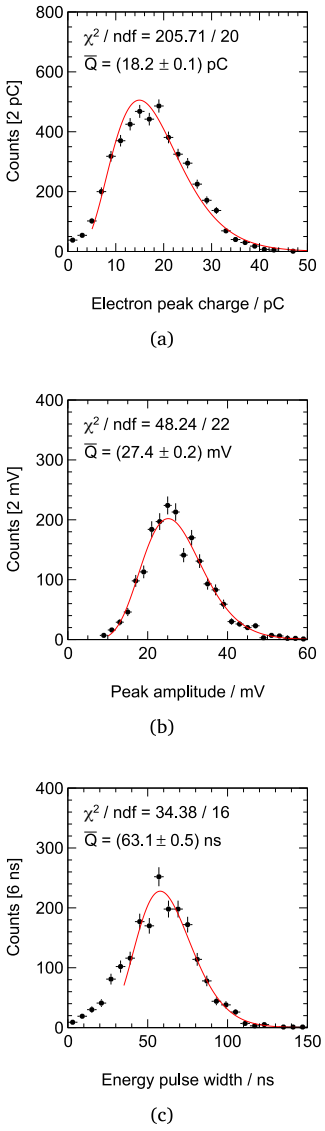

Fig. 14. Examples of the charge distribution, all recorded at cathode voltages of −520 V. (a) Electron peak charge, measured after the Cividec amplifier, (b) Peak amplitude of the FastIC's shaper output, (c) Energy pulse width of the FastIC's binary output. Fitted to the data is the Polya distribution (Eq. (1)).

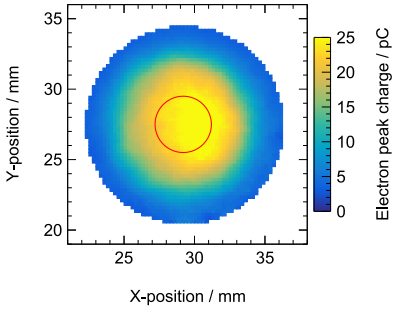

Fig. 15. Example of the geometrical cut, through which only events in the centre of the readout pad — indicated by the red circle — are selected.

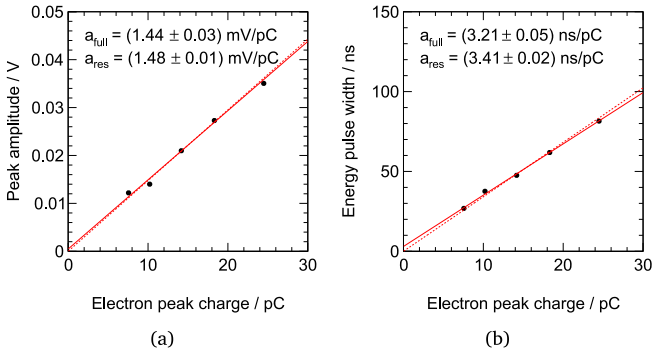

Fig. 16. Relation between the mean electron peak charge and the mean shaper peak amplitude (a) or the mean energy pulse width (b), respectively. In all cases, the mean value was extracted from the Polya fit to the charge distribution (Fig. 14). Fitted to the here shown points are two linear functions: the solid line represents a full linear function $f(x) = ax + b$, while the dashed line represents a restricted linear function $f(x) = ax$.

peak in the Picosec waveform with respect to the emulated waveform in combination with the pole-zero cancellation of the shaper.

In order to perform linearity tests using beam test data, pulse height distributions are used,[5] and the mean must be extracted by fitting it to a Polya distribution (Fig. 14):

$$p(x \mid S, \theta, \overline{Q}) = \frac{S}{\overline{Q}} \frac{(\theta+1)^{(\theta+1)}}{\Gamma(\theta+1)} \left(\frac{x}{\overline{Q}}\right)^{\theta} \exp\left(-(\theta+1)\frac{x}{\overline{Q}}\right). \quad (1)$$

Here, S is a scaling factor, θ is the shape parameter of the distribution and $\overline{Q}$ is the mean value of the distribution, i.e. the mean signal amplitude. To generate the Polya distribution, a subset of the recorded interactions is selected (Fig. 15): to ensure that all UV photons from the Cherenkov cone are contained within the active area and no charge information is lost, the particle trajectory information reconstructed with the triple-GEM detectors from the beam telescope is used, with only these interactions being selected whose position is within a 2 mm radius around the centre of the readout pad. The results are shown in Fig. 16. Fitted to the data points is a linear function, demonstrating that the Picosec waveform does not affect the charge processing in the FastIC.

[5] Given the experimental set-up, this had to be realised in three consecutive cathode voltage scans. First, the electron peak charge distributions were measured, with the additional amplifier being directly connected to the oscilloscope. Afterwards, the output of the amplifier was connected to the FastIC, with the distributions of the shaper output being measured in the second cathode voltage scan and the distributions of the energy pulse width on the third scan.

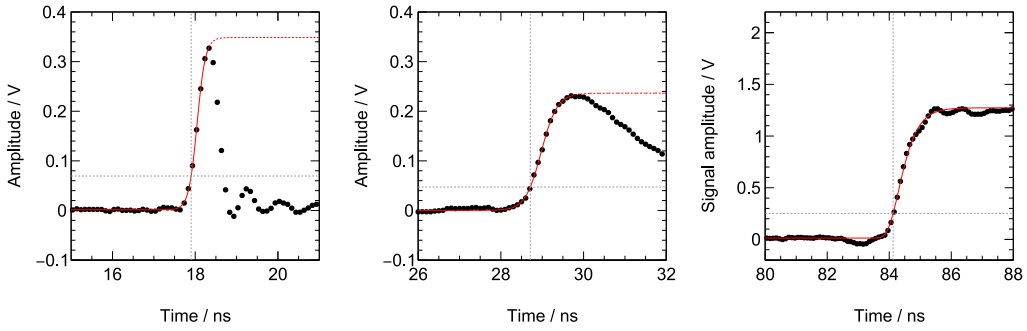

Fig. 17. Example of the sigmoid fit to (a) the MCP-PMT signal and (b) the Picosec waveform. In addition, (c) shows the sigmoid fit to a FastIC output signal.

7. Time resolution

To study the time resolution of the DUT, the time difference between the particles' measured signal arrival times obtained from the MCP-PMT and the DUT is taken. To determine the SAT, a Fermi-Dirac sigmoid function

$$f(x \mid S, k, x_0, a, h) = \frac{S}{\left(1 + e^{-k(x-x_0)}\right)^a} + h \tag{2}$$

is fitted to the rising edge of the MCP-PMT signal (Fig. 17(a)) and the rising edge of the electron peak (Fig. 17(b)), respectively, which serves as a reference measurement. The SAT is then defined as the 20 % point of the sigmoid fit, working as a Constant Fraction Discriminator (CFD). Since the FastIC data is acquired with an oscilloscope, the same analysis code is also used to determine the SAT from the binary signal (Fig. 17(c)).

Before generating the time difference distribution to determine the time resolution, a time walk correction is performed (Fig. 18). In the case of the reference data sets with the fit to the electron peak, this is necessary partially because of the jitter of the first ionisation taking place in the pre-amplification gap — the later this happens, the smaller the signal amplitude and vice versa [19]. Being a detector effect, this is also included in the FastIC data. However, here the main contribution arises from the timing-at-threshold of the preceding hardware processing of the signal, resulting in a much larger time walk of around 1 ns. Effectively, due to the timing-at-threshold, this time walk is the result from sampling the leading edge of the electron peak from the Picosec waveform with the THL of the electronics.

Fitted to the data is a reciprocal function

$$t(x \mid a, b, c) = a + \frac{b}{x^c}\ , \tag{3}$$

with the free parameters a, b and c. From this fit, the time walk correction can be applied via

$$\Delta t(x) = t_{\mathrm{SAT}}(x) - t(x \mid a, b, c)\ , \tag{4}$$

with t_{SAT} being the measured signal arrival time and $t(x \mid a, b, c)$ the result of the time walk fit.

After the time walk correction is applied, the time difference distribution is generated — an example distribution from the Cividec reference data is shown in Fig. 19 — representing the fluctuations of the time walk corrected data, i.e. the time resolution equals $\sigma_{\Delta t}$. Similar to the charge processing studies (Section 6.2), only the interactions recorded within the centre of the readout pad are used for it. The results, i.e. the time resolution depending on the cathode voltage and thus the pre-amplification factor, are shown in Fig. 20(a); the intrinsic time resolution of the MCP-PMT is still convoluted within them. It compares the reference data, measured with the Cividec amplifier and the standard waveform analysis, with the FastIC data. From the data,

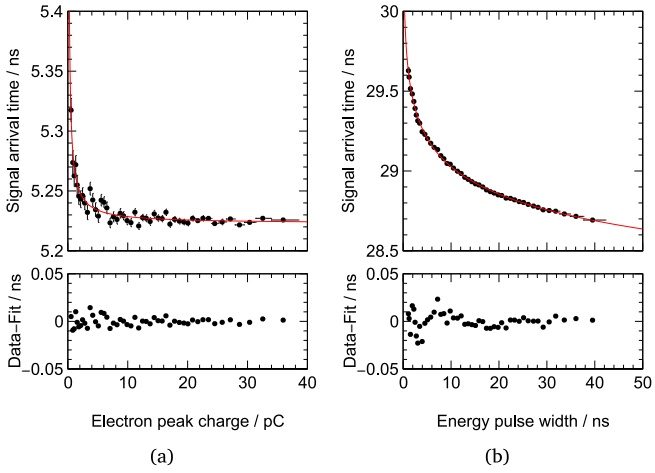

Fig. 18. Time walk of the SAT, depending on the signal charge for (a) the reference analysis and (b) the FastIC measurements.

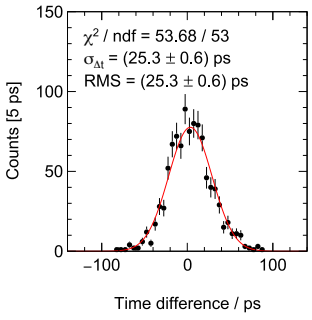

Fig. 19. Example of a time difference distribution, generated from the time walk corrected SATs of the MCP-PMT reference and the amplified Picosec signal. Fitted to the data is a Gaussian function. The distribution shown here belongs to the reference data set, taken with the Cividec amplifier and directly measured with the oscilloscope.

it becomes evident that the best time resolution which can be reached with FastIC and Picosec MM is around 50 ps.

This is however not related to intrinsic resolution effects of the FastIC, but to the timing-at-threshold and the subsequent time walk correction. In Fig. 20(a), also a data series (Cividec t@THL) is shown, where the default Picosec MM analysis was modified, with the CFD being replaced by a fixed threshold timing, mimicking the hardware behaviour of the FastIC. As it can be seen, the time resolution worsens, becoming compatible with the results from the FastIC.

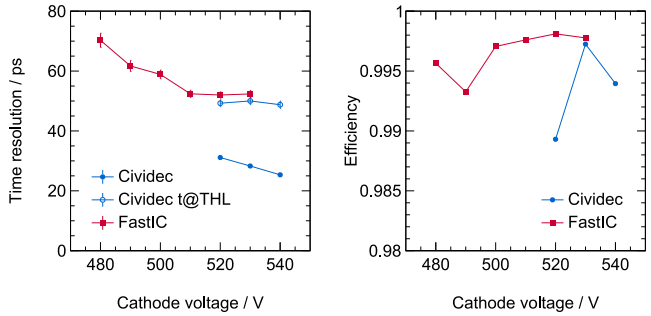

Fig. 20. (a) Resulting time resolution of the single-channel DUT, with Cividec amplifier and FastIC readout. In addition, the results for the Cividec amplifier with a software timing-at-threshold-level (t@THL) instead of using the software CFD are shown. (b) Efficiency of the single-channel DUT, with Cividec amplifier and FastIC readout. It should be noted that the uncertainties (around ±4 %) are not shown for the sake of improved clarity of the graphics.

8. Detector efficiency

In addition to the time resolution, the DUTs efficiency was studied, depending on the cathode voltage V_c. As the MCP-PMT serves as a trigger input for the readout and the data acquisition, the number of trigger signals N_t generated is the number of expected recorded interactions. This number is reduced by the geometrical cut, due to the area of the MCP-PMT being larger than the readout pads of the DUTs, as well as only signals within the centre of the readout pad being considered for the time resolution analysis. The cut is identical to the one for the energy analysis (Fig. 15), only that it is now applied to both, the MCP-PMT data and the DUT data. Thus, the efficiency is given as

$$\epsilon(V_c) = \frac{\widetilde{N}_{\mathrm{DUT}}(V_c)}{\widetilde{N}_t}\ , \tag{5}$$

with $\widetilde{N}_{\mathrm{DUT}}$ being the number of signals recorded within the geometrically accepted area of the DUT and $\widetilde{N}_t$ the number of trigger signals generated with the MCP-PMT[6] and the APV25/SRS trigger logic, also within the geometrically accepted area. The results are shown in Fig. 20(b). It can be seen that within the uncertainties, which are around ±0.04, the DUT has an efficiency of 1, independent of the readout anode and readout electronics.

9. Multi-channel readout

After characterising the readout from a Picosec MM with the FastIC, beam measurements with a multi-channel detector were performed to study the multi-channel readout capabilities. The analysis procedure has been kept identical to the single-channel test beam studies, including the extrapolation of the track points within the pads through the GEM telescope (see Section 6.2).

At first, the results from the energy branch (Fig. 21(a)) are studied. It can be seen that the average width of the energy pulse varies by up to 30 % between readout pads. This is caused by a convolution of variations between the readout pads of the detector [7,21], as well as variations between the front-end channels of the FastIC, which do not give the same shaper peak amplitude and thus energy pulse width for the same input charge, i.e. requiring dedicated charge calibrations for future measurements. The reduced energy pulse width at the edges of the pads is due to the Cherenkov cone not being fully contained

[6] In dedicated previous studies, it was found that the efficiency of the MCP-PMT within the selected region is > 95 % [20].

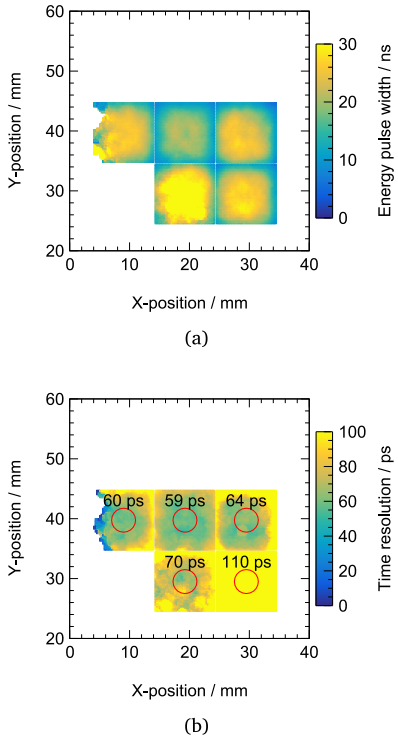

Fig. 21. Map of the pads read out with the FastIC. In (a), the measured amplitude (expressed as width of the energy pulse) is shown, while in (b), the time resolution is shown.

in the active area, i.e. the loss of charge information; the pads have been analysed individually without matching events shared between neighbouring pads.

In terms of time resolution, it can be seen that the response is more uniform than the charge measurement, also being compatible with the previous measurements. The achieved time resolutions between 60 to 70 ps are slightly worse than the one measured with a single channel. This can be attributed to a worse detector time resolution of around 40 ps, which was caused by a degraded CsI photocathode. The only significant exception for the time resolution behaviour can be seen in the lower right readout pad, where a time resolution of worse than 100 ps is measured. This was identified to be caused by one of the custom pre-amplifiers not working entirely correctly. These results show that FastIC can be indeed a valuable option for the multi-channel readout of Picosec MicroMegas detectors.

10. Conclusion and outlook

In the scope of this paper, the integration of the FastIC front-end ASIC and the Picosec MicroMegas detectors was studied in view of a multi-channel readout for fast-timing gaseous detectors. It was demonstrated that Picosec MM detectors can be successfully read out with the FastIC and that their combination is principally suitable for fast-timing applications. The electronic's energy processing preserves the charge information of the input waveforms. Time resolutions of 50 ps have been reached, being slightly larger than the intrinsic detector time resolutions. This is caused by the timing-at-threshold of the FastIC, leading to a time walk of around 1 ns of the signal arrival time. Also, the multi-channel readout performance was demonstrated, preserving the measured time resolutions. This is encouraging for further pursuit and improvement of the integration of FastIC and Picosec MM, especially with the FastIC+ ASIC that includes integrated digitisation. As such, the FastIC+ would for example enable uniformity measurements of the large area $10 \times 10\,\mathrm{cm}^2$ detector.

CRediT authorship contribution statement

L. Scharenberg: Writing – original draft, Investigation, Formal analysis. **J. Alozy:** Resources. **Y. Angelis:** Writing – review & editing. **S. Aune:** Resources. **R. Ballabriga:** Writing – review & editing, Validation, Resources, Project administration. **J. Bortfeldt:** Software. **F. Brunbauer:** Writing – review & editing, Software, Resources, Conceptualization. **M. Brunoldi:** Writing – review & editing. **M. Campbell:** Writing – review & editing, Supervision, Project administration, Funding acquisition. **J. Datta:** Writing – review & editing. **R. De Oliveira:** Resources. **K. Dehmelt:** Writing – review & editing. **G. Fanourakis:** Writing – review & editing, Conceptualization. **J.M. Fernandez-Tenllado:** Writing – review & editing, Resources. **K.J. Flöthner:** Writing – review & editing. **D. Fiorina:** Writing – review & editing. **M. Gallinaro:** Writing – review & editing, Funding acquisition. **F. Garcia:** Writing – review & editing, Project administration. **D. Gascon:** Writing – review & editing, Validation, Supervision, Project administration, Funding acquisition. **I. Giomataris:** Writing – review & editing, Conceptualization. **K. Gnanvo:** Writing – review & editing, Software, Funding acquisition. **S. Gomez:** Writing – review & editing, Validation, Software, Resources. **F.J. Iguaz:** Writing – review & editing. **D. Janssens:** Writing – review & editing. **A. Kallitsopoulou:** Writing – review & editing, Software, Resources. **M. Kovacic:** Writing – review & editing, Resources. **B. Kross:** Writing – review & editing, Resources. **P. Legou:** Writing – review & editing, Resources. **M. Lisowska:** Writing – review & editing, Software, Resources. **J. Liu:** Writing – review & editing, Project administration, Funding acquisition. **M. Lupberger:** Writing – review & editing, Resources. **R. Manera:** Writing – review & editing, Validation, Resources. **I. Maniatis:** Writing – review & editing. **A. Mariscal:** Writing – review & editing, Validation, Resources. **J. Mauricio:** Writing – review & editing, Resources. **J. McKisson:** Writing – review & editing. **Y. Meng:** Writing – review & editing. **H. Muller:** Writing – review & editing. **E. Oliveri:** Writing – review & editing, Supervision, Project administration, Funding acquisition, Conceptualization. **G. Orlandini:** Writing – review & editing. **A. Pandey:** Writing – review & editing. **T. Papaevangelou:** Writing – review & editing, Supervision, Project administration, Funding acquisition. **E. Picatoste:** Writing – review & editing, Resources. **M. Piller:** Writing – review & editing, Validation, Resources, Investigation. **M. Pomorski:** Writing – review & editing. **L. Ropelewski:** Writing – review & editing, Supervision, Project administration, Funding acquisition. **D. Sampsonidis:** Writing – review & editing, Supervision, Conceptualization. **A. Sanuy:** Writing – review & editing, Resources. **T. Schneider:** Resources. **E. Scorsone:** Writing – review & editing. **L. Sohl:** Software. **M. van Stenis:** Writing – review & editing, Resources. **Y. Tsipolitis:** Writing – review & editing, Resources. **S.E. Tzamarias:** Writing – review & editing, Supervision, Software, Project administration, Conceptualization. **A. Utrobicic:** Writing – review & editing, Software, Resources, Funding acquisition. **I. Vai:** Writing – review & editing, Project administration, Funding acquisition. **R. Veenhof:** Writing – review & editing, Conceptualization. **P. Vitulo:** Writing – review & editing. **X. Wang:** Writing – review & editing. **S. White:** Writing – review & editing, Supervision, Project administration, Conceptualization. **W. Xi:** Writing – review & editing. **Z. Zhang:** Writing – review & editing. **Y. Zhou:** Writing – review & editing, Resources, Project administration.

Declaration of competing interest

The authors declare that they have no known competing financial interests or personal relationships that could have appeared to influence the work reported in this paper.

Acknowledgements

This work has been supported by the CERN EP R&D Strategic Programme on Technologies for Future Experiments (https://ep-rnd.web.cern.ch/). The authors would like to thank the BE-CEM-EPR electronics services, in particular Pascal Vulliez, for the design and manufacturing of the SLVS-to-CMOS multi-channel readout adapter. Further, the authors would like to acknowledge the support by the RD51 collaboration, in the framework of RD51 common projects; the Cross-Disciplinary Program on Instrumentation and Detection of CEA, the French Alternative Energies and Atomic Energy Commission; the PHENIICS Doctoral School Program of Université Paris-Saclay, France; the Program of National Natural Science Foundation of China (grant number 11935014); the COFUND-FP-CERN-2014 program (grant number 665779); the Fundação para a Ciência e a Tecnologia (FCT), Portugal (CERN/FISPAR/0005/2021); the Enhanced Eurotalents program (PCOFUND-GA-2013-600382); the US CMS program under DOE contract number DE-AC02-07CH11359; the European Union's Horizon Europe research and innovation programme under grant agreement No. 101099896. This material is based upon work supported by the U.S. Department of Energy, Office of Science, Office of Nuclear Physics under contracts DE-AC05-06OR23177.

Data availability

Data will be made available on request.

References

[1] ECFA Detector R&D Roadmap Process Group, The 2021 ECFA Detector Research and Development Roadmap, Tech. rep., Geneva, 2020, http://dx.doi.org/10.17181/CERN.XDPL.W2EX, URL https://cds.cern.ch/record/2784893.

[2] ATLAS Collaboration, Technical Design Report: A High-Granularity Timing Detector for the ATLAS Phase-II Upgrade, Tech. rep., Geneva, 2020, URL https://cds.cern.ch/record/2719855.

[3] CMS Collaboration, A MIP Timing Detector for the CMS Phase-2 Upgrade, Tech. rep., Geneva, 2019, URL https://cds.cern.ch/record/2667167.

[4] F.J. Iguaz, et al., (Picosec MicroMegas Collaboration), PICOSEC: Charged particle timing at sub-25 picosecond precision with a Micromegas based detector, Nucl. Instrum. Methods Phys. Res. A 903 (2018) 317–325, http://dx.doi.org/10.1016/j.nima.2018.04.033.

[5] A. Utrobicic others, (Picosec MicroMegas Collaboration), A large area 100 channel Picosec Micromegas detector with sub 20 ps time resolution, J. Instrum. 18 (2023) C07012, http://dx.doi.org/10.1088/1748-0221/18/07/C07012.

[6] C. Aimè, et al., Fast timing detectors for the muon system of a muon collider experiment: requirements from simulation and prototype performance, J. Instrum. 19 (2024) C03052, http://dx.doi.org/10.1088/1748-0221/19/03/C03052.

[7] M. Lisowska, et al., (Picosec MicroMegas Collaboration), Towards robust PICOSEC Micromegas precise timing detectors, J. Instrum. 18 (2023) C07018, http://dx.doi.org/10.1088/1748-0221/18/07/C07018.

[8] D. Breton, et al., Measurements of timing resolution of ultra-fast silicon detectors with the SAMPIC waveform digitizer, Nucl. Instrum. Methods Phys. Res. A 835 (2016) 51–60, http://dx.doi.org/10.1016/j.nima.2016.08.019.

[9] Y. Meng, et al., PICOSEC Micromegas Precise-timing Detectors: Development towards Large-Area and Integration, Submitt. J. Instrum. (2025) http://dx.doi.org/10.48550/arXiv.2501.04991.

[10] S. Gómez, et al., FastIC: a fast integrated circuit for the readout of high performance detectors, J. Instrum. 17 (2022) C05027, http://dx.doi.org/10.1088/1748-0221/17/05/C05027.

[11] A. Mariscal-Castilla, S. Gómez, et al., Toward Sub-100 ps TOF-PET Systems Employing the FastIC ASIC With Analog SiPMs, IEEE Trans. Radiat. Plasma Med. Sci. (2024) http://dx.doi.org/10.1109/TRPMS.2024.3414578.

[12] S. Gómez, et al., FastIC: A Highly Configurable ASIC for Fast Timing Applications, in: 2021 IEEE Nuclear Science Symposium and Medical Imaging Conference (NSS/MIC), 2021, pp. 1–4, http://dx.doi.org/10.1109/NSS/MIC44867.2021.9875546.

[13] D. Sánchez, et al., HRFlexToT: A High Dynamic Range ASIC for Time-of-Flight Positron Emission Tomography, IEEE Trans. Radiat. Plasma Med. Sci. 6 (2022) 51–67, http://dx.doi.org/10.1109/TRPMS.2021.3066426.

[14] Y. Giomataris, Ph. Rebourgeard, J.P. Robert, G. Charpak, MICROMEGAS: a high-granularity position-sensitive gaseous detector for high particle-flux environments, Nucl. Instrum. Methods Phys. Res. A 376 (1996) 29–35, http://dx.doi.org/10.1016/0168-9002(96)00175-1.

[15] A. Utrobicic, Advancements in a large area 100 channel PICOSEC Micromegas detector module, 2022, Presentation at the RD51 Collaboration Meeting URL https://indico.cern.ch/event/1138814/contributions/4915978/.

[16] C. Hoarau, et al., RF pulse amplifier for CVD-diamond particle detectors, J. Instrum. 16 (2021) T04005, http://dx.doi.org/10.1088/1748-0221/16/04/T04005.

[17] C. Altunbas, et al., Construction, test and commissioning of the triple-gem tracking detector for compass, Nucl. Instrum. Methods Phys. Res. A 490 (2002) 177–203, http://dx.doi.org/10.1016/S0168-9002(02)00910-5.

[18] S. Martoiu, et al., Development of the scalable readout system for micro-pattern gas detectors and other applications, J. Instrum. 8 (2013) C03015, http://dx.doi.org/10.1088/1748-0221/8/03/C03015.

[19] J. Bortfeldt, et al., Modeling the timing characteristics of the PICOSEC Micromegas detector, Nucl. Instrum. Methods Phys. Res. A 993 (2021) 165049, http://dx.doi.org/10.1016/j.nima.2021.165049.

[20] L. Sohl, Spatial time resolution of MCP-PMTs as a t_0-reference, Nucl. Instrum. Methods Phys. Res. A 936 (2019) 583–585, http://dx.doi.org/10.1016/j.nima.2018.11.138.

[21] M. Lisowska, Towards robust PICOSEC Micromegas precise timing detectors, in: 7th International Conference on Micro Pattern Gaseous Detectors, 2022, URL https://indico.cern.ch/event/1219224/contributions/5130512/.